Evaluation of Charge Mobility in Organic Materials: From Localized to Delocalized Descriptions at a First-Principles Level

Zhigang Shuai, Linjun Wang, and Qikai Li*

The carrier mobility for carbon electronic materials is an important parameter for optoelectronics. We report here some recently developed theoretical tools to predict the mobility without any free parameters. Carrier scatterings with phonons and traps are the key factors in evaluating the mobility. We consider three major scattering regimes: i) where the molecular internal vibration severely induces charge self-trapping and, thus, the hopping mechanism dominates; ii) where both intermolecular and intramolecular scatterings come to play roles, so the Holstein-Peierls polaron model is applied; and, iii) where charge is well delocalized with coherence length comparable with acoustic phonon wavelength, so that a deformation potential approach is more appropriate. We develop computational methods at the first-principles level for the three different cases that have extensive potential application in rationalizing material design.

1. Introduction

The charge mobility in organic materials is the essential parameter in determining electronic device performance.[1] Literally, it means the ability of a charge to move in the bulk material. With the presence of an electric field, F, an electron acquires an additional momentum $\Delta q = -eFt$ for a time period t. According to the classical Boltzmann transport picture, the scattering of electrons due to impurities, defects, and lattice vibrations tends to restore the electron momentum to its original value (the relaxation time approximation). Thus, in the steady current condition, $\Delta q = -eF\tau$ where τ is the mean scattering time, i.e., the average time between two consecutive scattering events. If the charge has an effective mass $m*$, the velocity becomes $v = -\frac{e\tau}{m*}F$, where the prefactor is defined as the mobility $\mu = -\frac{e\tau}{m}$. A silicon single crystal possesses a charge mobility ranging from a few hundreds to a few thousands $cm^2\ V^{-1}\ s^{-1}$ at room temperature.[2] For new carbon materials, such as single-wall carbon nanotubes (SWNT) or graphene sheets (GS), the mobility can reach a few hundred thousand $cm^2\ V^{-1}\ s^{-1}$.[3] Its large mobility, as well as natural abundance and stability, make silicon the most prominent electronic material. SWNTs or GS are very promising for the next generation of electronics because of their huge mobilities. Organic materials usually have much lower mobility and poorer stability and, thus, are not destined to replace silicon. However, due to their processability and flexibility, among other advantages, organic materials can play an important role in next-generation electronic applications, such as large area and flexible devices.[4] Designing new materials with large mobility has been a formidable task in the past two decades and now a dozen molecular systems have been demonstrated to exhibit room temperature mobilities of between 1 and 10 $cm^2\ V^{-1}\ s^{-1}$[5] in thin film forms and even larger mobilities for single-crystal forms.[6]

The transport in organic materials has been a subject of theoretical interests for almost sixty years. Holstein proposed the small polaron model in 1959, which depicted a general scheme for electron motion in organic solids.[7] However, there are at least three reasons for the recent renaissance in theoretical interest: i) there have been great advances made in recent years both in synthesis of better performed molecules and in materials processing; ii) tremendous advances in electronic structure theory and computational technology have allowed a quantitative description to be developed for the charge mobility in molecular crystals; and, iii) despite numerous theoretical studies having been made in the past, the comparison between experiment and theory based on ultrapure single crystals had been always extremely difficult due to lack of quantitative calculations as well as the disorder/impurity often present in molecular materials. Thus, it is difficult to judge the applicability of the approximations often applied at different levels to solve the Holstein model

Prof. Z. Shuai
Key Laboratory of Organic OptoElectronics and Molecular Engineering
Department of Chemistry
Tsinghua University, 100084 Beijing, PR China
E-mail: zgshuai@tsinghua.edu.cn
Dr. L. Wang
Key Laboratory of Organic OptoElectronics and Molecular Engineering
Department of Chemistry
Tsinghua University, 100084 Beijing, PR China
Dr. Q. Li
Key Laboratory of Organic Solids
Beijing National Laboratory for Molecular Science (BNLMS) Institute of Chemistry
Chinese Academy of Sciences, 100190 Beijing, PR China

DOI: 10.1002/adma.201003503

Hamiltonian. These facts have hindered our understanding of the transport mechanism.

On the other hand, organic devices have often been described by phenomenological disorder models. The most successful model was developed by Bässler and coworkers, assuming static disorder in the site energy and charge hops between sites through absorbing or emitting phonons.[8] In such a model, the distribution of site energy is fully random, obeying a Gaussian distribution. This model was later modified using a correlated energetic disorder to account for more realistic situation with charge–dipole interaction.[9] This model has been very successful in describing both the temperature and field dependence for the mobility in organic devices.

Nevertheless, from the point of view of material design, a microscopic model for the intrinsic property is highly desirable. Defects and impurities can be minimized through both molecular design and material processing. Approximately, different scattering relaxation times can be added up as: $\frac{1}{\tau} = \frac{1}{\tau_{op}} + \frac{1}{\tau_{ac}} + \frac{1}{\tau_{imp}} + \cdots$. Thus, the shortest relaxation time contributes the most to the mobility. The relaxation time attributable to impurities is extrinsic, dependent on the type. There has been strong interest in determining what the intrinsic mobility arising from scatterings with phonon is for a given material. There are two transport pictures: the band model for delocalized electrons and the hopping model for localized charge. Experimentally, evidence has been found that, in polyacenes and rubrene single crystals, a band picture is more appropriate.[10] Significant progress has been achieved in recent years in a number of areas, for example: i) based on semiclassical Marcus electron transfer theory and first-principles calculations, molecular parameters relevant to charge transport have been explored by Brédas and coworkers[11] by investigating the intermolecular coupling and the molecular reorganization energy as well as the polarization energy in the bulk;[12] ii) Munn and Silbey developed a variational approach to the Holstein model and compared the local and non-local linear electron–phonon coupling contributions to band and hopping behaviors[13] – they concluded that the non-local term tends to enhance the hopping behavior; iii) Kenkre and coworkers derived a working expression for the mobility by assuming a direction-dependent local electron–phonon coupling constant, in which non-local coupling was also considered;[14] iv) Bobbert and coworkers generalized the Holstein model to the Holstein–Peierls model by including non-local electron–phonon coupling terms, which are evaluated by DFT while assuming the molecule itself is a rigid body;[15] and, v) a time-dependent Schrödinger equation with a Su–Schrieffer–Heeger Hamiltonian has been solved numerically for the charge diffusion process with local electron–phonon coupling by Hultell and Stafström[16] and with non-local electron–phonon coupling by Troisi and Orlandi,[17] where phonons are treated classically.

Here, we summarize recent progress made in our group towards better understanding of charge transport in organic materials and quantitative predictions of carrier mobility through first-principles calculations. We classify the electron–phonon interaction into three categories, for each of which we have developed theoretical methods. In the first category,[18] the electron interacts strongly with intramolecular vibrations which eventually lead to self-localization. Namely, the intermolecular electron coupling (V) is much less than the molecular reorganization energy (λ).[19–22] Each molecule acts as a charge trap. It is thus appropriate to apply Marcus theory to calculate the intermolecular charge transfer rates. A more elaborate and appropriate description is to consider nuclear tunneling effects to account the quantum nature of molecular vibration.[23] Next, the charge diffusion is modeled through a random walk numerical simulation, much as in the phenomenological disorder model.[24] Since the molecular parameters enter explicitly into evaluation of the charge diffusion constant, this approach is really at multiscale, allowing molecular design for high charge mobility. In this case, it is found that the dynamic disorder does not play an essential role for charge transport in higher than one space dimension.[25] In the second category, where V is comparable to λ, and the localized picture should not be imposed at first-hand, we consider the Holstein–Peierls model, where both intra- and inter-molecular vibrations are considered to be linearly coupled with electrons.[26] All the parameters in the Hamiltonian are evaluated through DFT calculations, allowing us to establish quantitative structure-property relationship and predictions. Both pressure- and temperature-dependent structures have been taken into account.[27,28] In the third category, the coherent length of electrons is assumed to be very long, matching the wavelength of acoustic phonons, much as in inorganic semiconductors. In this case, the scattering process is modeled by a deformation potential formalism implemented in DFT calculations.[29] Typical examples are shown for the graphene nanoribbon.[30]

2. Intermolecular Hopping Description

In the strong electron–phonon coupling limit, upon charging a molecule undergoes a large geometry relaxation, which eventually traps the charge. Then the small polaron transport can be viewed as intermolecular charge hopping,[31] falling well into the Marcus electron transfer regime with $V \ll \lambda$. Here, the electron transfer rate between two identical molecules is:

$$k = \frac{V^2}{\hbar}\left(\frac{\pi}{\lambda k_B T}\right)^{1/2} \exp\left(-\frac{\lambda}{4k_B T}\right) \quad (1)$$

The electron coupling V can be evaluated directly through the diabatic model:[19,32]

$$V = < \phi^{0,a} \mid F \mid \phi^{0,b} > \quad (2)$$

Here, $\phi^{0,a}$ and $\phi^{0,b}$ represent the highest occupied molecular orbitals (HOMOs) or the lowest unoccupied molecular orbitals (LUMOs) of isolated molecules a and b for holes or electrons, respectively. F is the Fock operator for the non-interacting dimer: $F = SC\varepsilon C^{-1}$, where S is the intermolecular overlap matrix, C and ε are the molecular orbital coefficients and the eigen values from the one-step diagonalization without iteration. This approach is simple and reliable, and most importantly, it can effectively avoid the fictitious contribution from site-energy difference when the two molecules are not equivalent, for instance, not fully cofacially packed.[21]

The reorganization energy λ can be evaluated through the adiabatic energy potential surface.[24] Suppose the initial state

is $|M_a\ M_b^+>$ and the final state is $|M_a^+ M_b>$. Namely, molecule a (b) accepts (donates) one positive charge. The internal reorganization energy consists of two parts: the relaxation energy for a from a neutral to a charged geometry, and the relaxation energy for b from a charged to a neutral geometry. Another way to visualize this process is the vibration mode softening or stiffening. The reorganization energy is a sum of all the mode relaxation energies. Both ways give almost identical results,[24,33] indicating that the harmonic oscillator model works well for molecular charging process.

Based on V and λ only, some material design strategies have already been devised.[20,22,34–36] For example, in the case of triphenyl amine dimer, theoretical calculations indicated that the dimer formed in macrocycle possesses a hole mobility of around 2×10^{-2} cm^2 V^{-1} s^{-1}, while the dimer in a linear chain has a hole mobility of around 2×10^{-3} cm^2 V^{-1} s^{-1}, in quantitative agreement with the experiments.[20] Here, V is only a few meV in both cases, while λ is 0.17 and 0.32 eV, respectively, well justifying the applicability of Marcus theory. The difference in mobility origins from the fact that the macrocyclic structure is more stabilized upon charging than the linear chain, i.e., λ is smaller for the former.

Marcus theory alone is not enough to give comprehensive description for charge transport, since the mobility is a bulk parameter. We proposed a random walk scheme to simulate the charge diffusion.[24] First, the molecular crystal structure is obtained either from experiment or from molecular mechanics simulation. An arbitrary molecule within the bulk is initially identified as the starting point. The probability for the charge to hop to its α-th neighbor is $p_\alpha = k_\alpha / \sum_\alpha k_\alpha$, where k_α is the electron transfer rate to the α-th neighbor. To decide the next site for the charge to land in, a random number r uniformly distributed between 0 and 1 is generated. If $\sum_{\beta=1}^{\alpha-1} p_\beta < r < \sum_{\beta=1}^{\alpha} p_\beta$, the charge moves to the α-th neighbor site with a hopping time $1/k_\alpha$ (see **Figure 1a**). The simulation keeps going until the diffusion distance exceeds at least 10^2–10^3 times the lattice constant. Following the same process, thousands of simulations should be performed to get a linear relationship between mean-square displacement and simulation time. A typical time evolution of the mean-square displacement is shown in Figure 1b. The diffusion constant is evaluated as $D = \frac{1}{2n} \lim_{t\to\infty} \frac{\langle r^2 \rangle}{t}$, where n is the space dimension. Then the mobility can be calculated with the Einstein relationship:

$$\mu = \frac{e}{k_B T} D \tag{3}$$

As an example of application, we tried to quantitatively understand the molecular size and packing effects on charge mobility for oligothiophenes (nT, n = 2–8), which were among the first OFET systems.[37] The molecular size is well-defined in terms of number of thiophene rings. Depending on the sublimation temperatures, 4T and 6T exhibit two different herringbone packings: with two molecules in one unit cell (Z = 2) for high temperature (HT) phase, and four molecules (Z = 4) in one unit cell for low temperature phase (LT).[38] 2T belongs to the HT phase, while 7T and 8T belong to the LT phase. In addition, for 3T, there are 8 molecules in one unit cell. Thus, various crystal structures also provide an ideal system to study the molecular packing effects on the mobility. Previous experiments have given the hole mobility in the range 2×10^{-7} to 0.3 cm^2 V^{-1} s^{-1}.[39] The intrinsic charge mobility is difficult to obtain, since it depends strongly on how the materials are prepared and how the devices are made. Nevertheless, theoretical results can provide reference values, shedding more fundamental insights. In Figure 1c, we depict the calculated room temperature hole mobility as a function of the molecular size and the crystal phase. For the same phase, the mobility increases with the molecular size because their V values are quite close while λ monotonously decreases with n.[24,33] Besides, the Z = 2 phase leads to a larger mobility than that of Z = 4 because the former has higher V due to better orbital overlap.[24] Note that the theoretical prediction indicates that from HT to LT, the hole mobility of 6T decreases from 0.025 to 0.0075 cm^2 V^{-1} s^{-1}, in good agreement with the experimental mobilities from 0.025 to 0.002–0.009 cm^2 V^{-1} s^{-1}.[40]

The hopping description described above is workable for the class of molecular materials with $V \ll \lambda$, where the electron–phonon scattering stems from the intramolecular vibrations and V is assumed to be constant. At room temperature, it is obvious that the relative orientation of molecules fluctuates all the time since the intermolecular interaction is van der Waals type weak, and thus V also fluctuates. What is the effect of these intermolecular vibrations? We simulated the molecular dynamics for a pentacene crystal with COMPASS force field,[41] which can describe reasonably the intermolecular interactions.[25] It was found that V follows a Gaussian distribution with the square of standard deviation $\sigma^2 \propto T$. At room temperature, the deviation of V is comparable to V itself. However, it is found that the mobility is insensitive to the fluctuation of V for the 2D herringbone sheet of pentacene. If we only consider a 1D stack, the mobility is reduced by about half, see Figure 1d.[25]

The conclusion of this section is that for molecular materials with $V \ll \lambda$, the charge transport can be well modeled by hopping mechanism and the charge mobility can be predicted from first-principles calculations coupled with electron transfer theory and a random walk simulation. In such circumstances, the intermolecular phonon scatterings do not play an appreciable role.

3. Holstein–Peierls Description

The Holstein–Peierls model is a more general description for charge transport in molecular crystal. The Hamiltonian reads:

$$H = \sum_{mn} \varepsilon_{mn} a_m^+ a_n + \sum_\lambda \hbar\omega_\lambda \left(b_\lambda^+ b_\lambda + \frac{1}{2} \right) + \sum_{mn\lambda} \hbar\omega_\lambda g_{\lambda mn} \left(b_\lambda^+ + b_{-\lambda} \right) a_m^+ a_n \tag{4}$$

Here, the operators $a_m^{(+)}$ and $b_\lambda^{(+)}$ represent annihilating (creating) an electron at molecule m with energy ε_{mm} and a phonon with mode λ of frequency ω_λ, respectively. $g_{\lambda mn}$ is the dimensionless electron–phonon coupling constant, including the inter- and intra-molecular vibrations scattering with local onsite energy ε_{mm} and non-local transfer integral ε_{mn} ($m \neq n$). Note

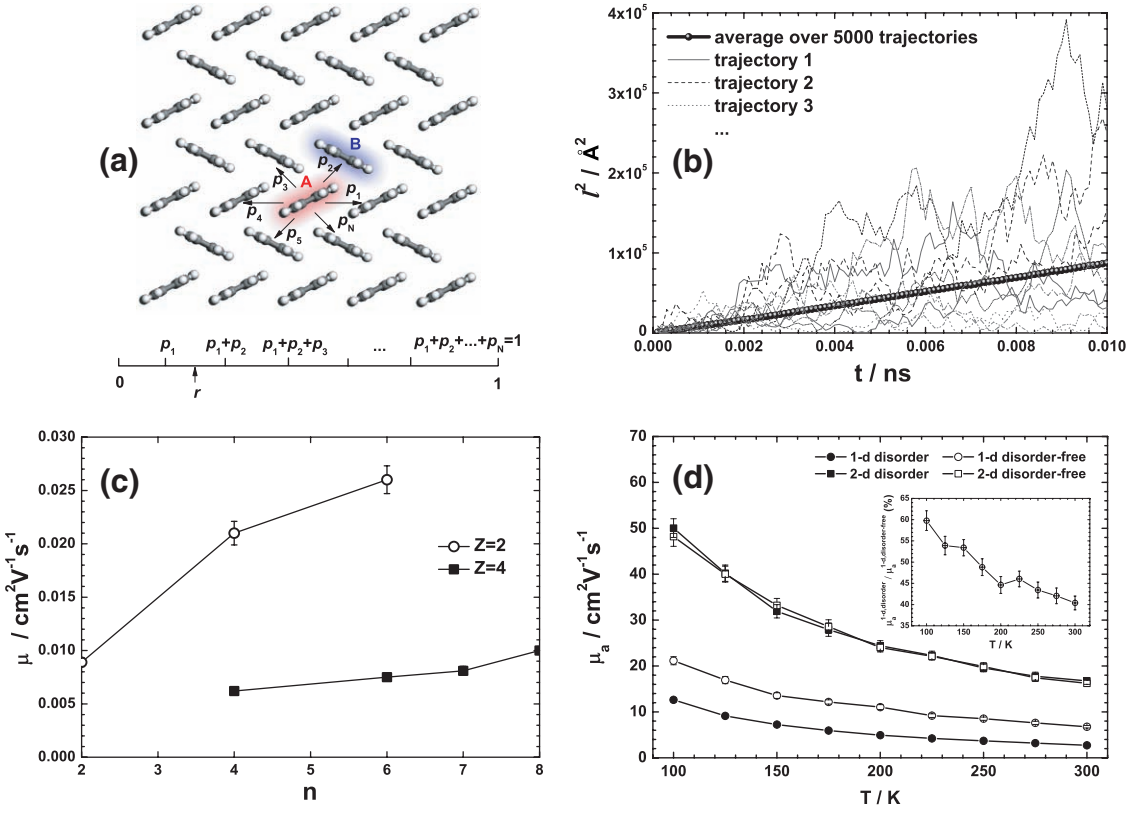

Figure 1. a) Top: schematic representation of the charge hopping pathways from molecule A to all its neighbors with probabilities p_1, p_2, …, p_N, where N is the number of neighbors. Bottom: a unit length is divided into N parts accrording to each probability, and a uniformly distributed random number, r, is generated. This determines which path is chosen for charge hopping, e.g., to molecule B if $p_1 < r < p_1 + p_2$. b) Time-dependent squared displacement for hole transport in a 2D pentacene layer. Each thin solid line represents an individual trajectory of the random walk simulation. The thick dotted line is the average over 5000 independent trajectories. c) Simulated hole mobility vs. the number of thiophene rings for oligothiophenes. d) Temperature-dependent hole mobility along the *a*-axis with and without dynamic disorder in 1D (circles) and 2D (squares); the ratio between the mobility with and without dynamic disorder in the 1D case is also shown in the inset. Panel (a) reproduced with permission.[18] Copyright 2010, RSC. Panel (c) reproduced with permission.[24] Copyright 2010, RSC. Panels (b) and (d) reproduced with permission.[25] Copyright 2010, RSC.

that in the hopping description, only the intra-local term is considered. Such a many-body Hamiltonian lacks an exact solution and approximations must be used.[42] Recent noteworthy progress includes the studies by Kenkre and coworkers[14] and Bobbert and coworkers.[15] After canonically transforming the electron–phonon Hamiltonian into a polaron plus distorted phonon, in particular applying thermal averages for higher-order terms and using the linear response approximation, the charge mobility can be expressed as:

$$\mu_\alpha(T) = \frac{e_0}{2k_B T\hbar^2} \sum_{n\neq m} (R_{\alpha m} - R_{\alpha n})^2 \int_{-\infty}^{\infty} dt e^{-\Gamma^2 t^2 - \sum_\lambda 2G_\lambda[1+2N_\lambda - \Phi_\lambda(t)]} \times \left[\varepsilon_{mn}^2 + (\varepsilon_{mn} - \Delta_{mn})^2 + \frac{1}{2}\sum_q (\hbar\omega_q g_{qmn})^2 \Phi_q(t)\right] \quad (5)$$

Where $R\alpha_m$ is the Cartesian coordinate of lattice site m in the α-th direction, Γ is a phenomenological parameter for inhomogenous line broadening, $G_\lambda = g_{\lambda mm}^2 + \frac{1}{2}\sum_{k\neq m} g_{\lambda mk}^2$ is athe effective electron–phonon coupling constant, $N_\lambda = 1/(e^{\hbar\omega_\lambda / k_B T} - 1)$ is the phonon occupation number, $\Phi_\lambda(t) = (1+N_\lambda)e^{-i\omega_\lambda t} + N_\lambda e^{i\omega_\lambda t}$ is the incoherent scattering factor, and $\Delta_{mn} = \frac{1}{2}\sum_\lambda \hbar\omega_\lambda \left[g_{\lambda mn}(g_{\lambda mm} + g_{\lambda nn}) + \frac{1}{2}\sum_{k\neq m,n} g_{\lambda mk} g_{\lambda kn}\right]$.

In principle, Equation (5) is quite general: it contains both the hopping and band mechanisms. When $g \gg 1$, the high-temperature approximation can be applied, then Equation (5) becomes the classical Marcus theory described above. When $g \ll 1$, Equation (5) becomes the band description.

We performed the first numerical study considering all the electron–phonon couplings at the DFT level for naphthalene crystals,[26–28] which have been extensively studied by Karl in purifying the samples and carrying out transport measurements over four decades.[43] The computational workhorse is the Vienna *ab initio* Simulation Package (VASP),[44] The Perdew–Burke–Ernzerhof (PBE) exchange-correlation (XC) functional[45] was chosen because it works better for molecular crystals than other functionals.[46] Geometry optimization is performed with a fixed lattice constant at the experimental level[47] due to the difficulty in handling weak intermolecular potential with DFT. The phonon modes are evaluated only at the Γ-point. The DFT band structure projected to the tight-binding model is used to fit all the ε_{mn} by a least-square minimization. For each optical phonon mode, we distort the molecular crystal along the normal coordinate with a small amplitude, and fit ε_{mn} for the distorted geometry, and then evalutate $g_{\lambda mn}$ as the

first-order derivative with respect to normal mode coordinates. We find that the intermolecular vibrations (with low frequencies) possess larger couplings (see **Figure 2a**). The electron–intramolecular phonon couplings in the crystal are found to be consistent with the calculation for a single molecule,[48a] indicating the intermolecular interaction does not affect appreciably the electron–intramolecular couplings. Upon applying pressure to naphthalene crystals, the charge mobility increases because of enhancement in ε_{mn} and reduction in $g_{\lambda mn}$ (see Figure 2b).

The most interesting feature based on the Holstein–Peierls model is the description of temperature dependence, which reveals the underlying transport mechanism. The temperature dependence of mobility for hole along the *a* direction in naphthalene single crystal is depicted in Figure 2c. Since the typical $g_{\lambda mn}$ for hole in naphthalene is less than 1, the calculated charge mobility as a function of temperature is typically band-like. It is of interest to note that along the *c'*-direction, the electron transport shows a band-hopping crossover behavior: at low temperature, the mobility decreases with *T*, showing a band-like behavior, and then, when the temperature reaches about 153 K, it levels off and starts to increase, much as for the hopping picture, see Figure 2d. This result agrees well with the experimental band-hopping transition temperature of 100–150 K.[48b] In this case, the contributions from hopping and from band are competitive since $g_{\lambda mn}$ for electrons in naphthalene is relatively large and ε_{mn} along the *c'*-direction is quite small.[26] Note that we have considered temperature-dependent crystal structures from experiments plus a few points from extrapolations here. If the temperature-dependent crystal structure is not considered, the crossover temperature would be as low as 23 K.[28]

Even though the Holstein–Peierls model can well describe the temperature dependence of mobility, it does not give quantitatively predictive values. For instance, the room temperature hole mobility along the *a*- or *b*-axes is calculated to be around 100 $cm^2\ V^{-1}\ s^{-1}$ (with a diminishingly small damping factor $\hbar\Gamma = 0.1$ meV), which is about one to two orders of magnitude larger than the experimental mobility obtained by Karl. Such overestimation can be ascribed to a number of factors: i) the neglect of acoustic phonon scatterings, which can be important for delocalized electrons; in the next section, we will present a study employing a deformation potential approach to take acoustic phonon scattering into accounts; ii) only the gamma-point of phonons is considered: for molecular crystals, there are usually large numbers of atoms in one unit cell and present computational capacity does not allow consideration of phonon dispersion; and, iii) the dephasing factor ($\hbar\Gamma = 0.1$ meV) is chosen only based on the consideration of convergence of

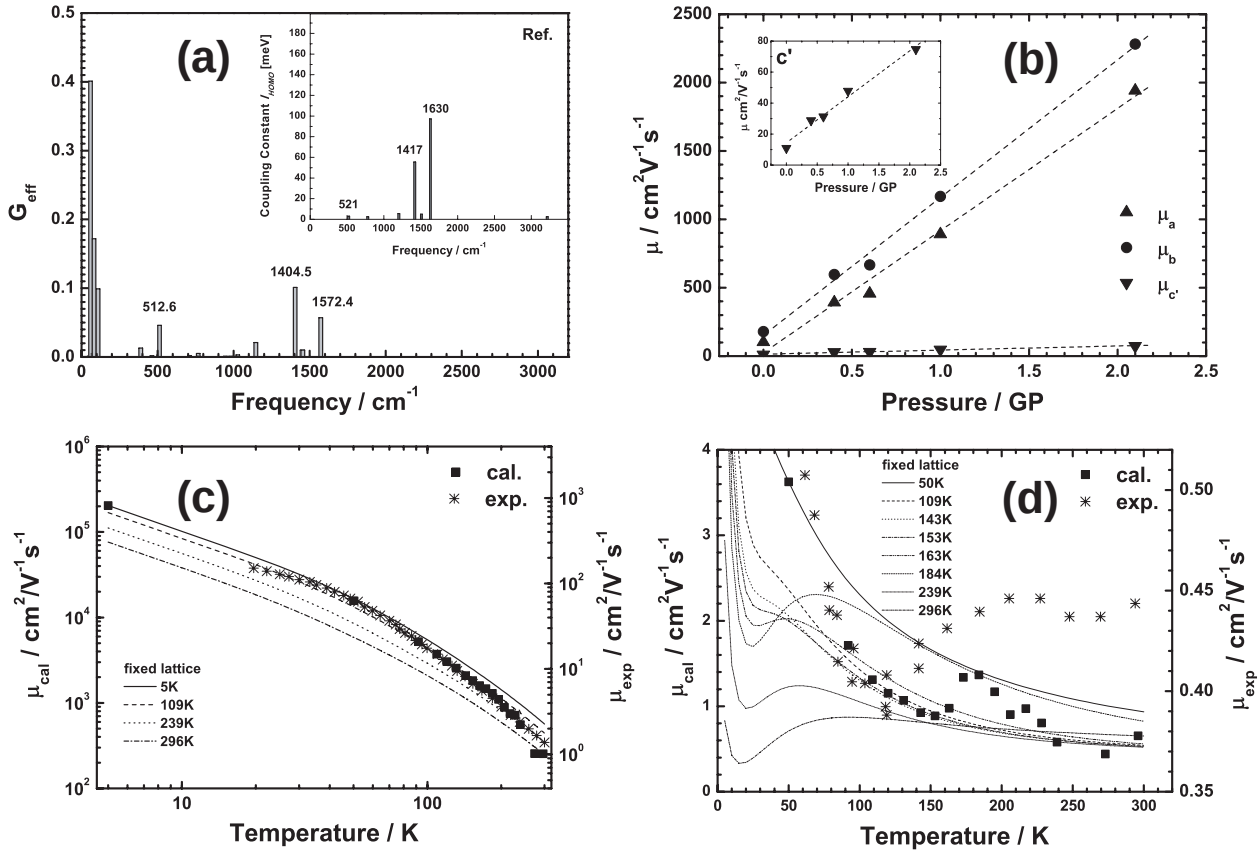

Figure 2. a) Effective coupling constants vs. phonon energies for HOMO of a naphthalene crystal. The single molecular calculation by Kato and Yamabe[48a] is shown in the inset. b) The relationship between the calculated hole mobilities and pressure for naphthalene crystal. The case along the c′-axis is shown in the inset for better visualization. c and d) The calculated and experimental results[43] of the temperature-dependent mobilities of hole in the *a*-axis and electron in the c′-axis, respectively. Reproduced with permission.[26,28] Copyright 2007/2008, ACS.

numerical integration in Equation (5), which must be very small in order to reveal the intrinsic behavior from the Holstein-Peierls model, but is too small to account for any impurity or disorder presented in real materials. Having stated these deficiencies, this work does represent the first attempt to incorporate a modern first-principles (parameter-free!) method for the polaron transport model.

4. Deformation Potential Theory

The deformation potential theory is a somewhat dated method proposed by Bardeen and Shockley in 1950 to describe the charge transport in inorganic semiconductors like silicon single crystals.[49] It was argued that the electron velocity with energy k_BT is about 1 nm s^{-1} at room temperature and the corresponding de Broglie wavelength is about 7 nm, much larger than the lattice constant, and thus the electron scatters mainly with acoustic phonons. Using the Boltzmann transport theory together with the relaxation time approximation, the electron (hole) mobility can be expressed as:[50a]

$$\mu_{\alpha}^{e(h)} = \frac{e}{k_B T} \frac{\sum_{i \in CB(VB)} \int \tau_{\alpha}\left(i, \vec{k}\right) v_{\alpha}^{2}\left(i, \vec{k}\right) \exp\left[\mp \frac{\varepsilon_i\left(\vec{k}\right)}{k_B T}\right] d\vec{k}}{\sum_{i \in CB(VB)} \int \exp\left[\mp \frac{\varepsilon_i\left(\vec{k}\right)}{k_B T}\right] d\vec{k}} \quad (6)$$

Here, the Boltzmann distribution is used for simplicity, CB (VB) expresses the conduction (valence) band, $\tau_{\alpha}(i,\vec{k}) = 1/\sum_{\vec{k}' \in BZ} \left\{ \frac{2\pi}{\hbar} \left| M_i\left(\vec{k}, \vec{k}'\right) \right|^2 \delta\left[\varepsilon_i\left(\vec{k}\right) - \varepsilon_i\left(\vec{k}'\right)\right] \left[1 - \frac{v_{\alpha}\left(i,\vec{k}'\right)}{v_{\alpha}\left(i,\vec{k}\right)}\right] \right\}$ is the scattering time for the electron in the i-th band with momentum $\vec{k}$,[50b] $\varepsilon_i(\vec{k})$ is the band dispersion, $\vec{v}\left(i,\vec{k}\right) = \nabla \varepsilon_i\left(\vec{k}\right)/\hbar$ is the electron group velocity, and $M_i\left(\vec{k},\vec{k}'\right)$ is the scattering matrix element for the electron in the i-th band from state $\vec{k}$ to $\vec{k}'$. In the low concentration limit, we can assume that $\left|M_i\left(\vec{k},\vec{k}'\right)\right|^2$ is momentum independent and can be evaluated with its mean value $\left\langle \left| M_i\left(\vec{k},\vec{k}'\right)\right|^2 \right\rangle = k_B T \left(E_1^i\right)^2 / C_{\beta}$, where C_{β} is the elastic constant along the β-th direction. If the effective mass approximation is applied, the mobility becomes solvable analytically:[49]

$$\mu = \frac{e\tau}{m^*} = \frac{(8\pi)^{1/2} e\hbar^4 C_{\beta}}{3m^{*5/2}(k_B T)^{3/2} E_1^2} \quad (7)$$

Here, $m^* = \hbar/[\partial^2 \varepsilon(k)/\partial k^2]$ is the effective mass, and $E_1 = \Delta E/(\Delta l/l_0)$ is the deformation potential, determined by the shift in the bottom position of CB or in the top position of VB, ΔE, with respect to the primitive cell length dilation $\Delta l/l_0$. Equation (7) is widely used, especially for 1D systems, such as linear polymers,[51] DNA strands,[52] carbon nanotubes[53] and graphene nanoribbons.[30] It should be noted that for graphene sheets or for the zig-zag graphene nanoribbons, due to the Dirac point or the edge state at the Fermi surface, the effective mass approximation fails and one needs to evaluate Equation (6) directly.

As an example, we tried to estimate the mobility in 1D graphene nanoribbon. Graphene presents plenty of new physics, promises many novel application potentials and represents one of the most exciting recent progressions in the material sciences.[54] For application in electronics, graphene possesses large mobility.[55] The two types of nanoribbons are sketched in **Figure 3a**, namely, the armchair graphene nanoribbon (AGNR) and zig-zag graphene nanoribbon (ZGNR). To avoid any dangling bonds, the edge carbons are all passivated with hydrogens. Geometry optimization and band structure are calculated by DFT with PBE functional within VASP. Note that the carbon 1s orbital is chosen as the energy reference, since it is not sensitive to the slight lattice expanding or shrinking, thus eliminating any artifact of the different energy origin at different lattice constant.

The ZGNRs are gapless due to the midgap state from the edge, therefore the main focus of study is the AGNRs, which possess finite band gaps. Hereafter the abbreviation N-AGNR is used to denote the AGNR with N carbon atoms along the side edge (see Figure 3a). It is found that the calculated effective mass for N-AGNR (N = 9–44) is within the range of 0.057–0.077 m_e, in close agreement with the experimental value of 0.06 m_e for graphene.[54] Since the electronic structure of N-AGNR exhibits a periodicity of 3, i.e., the edge of phenyl ring, we only show the band structure of three typical N-AGNRs in Figure 3b. For $N = 3M$ and $N = 3M + 1$. where M is an integer, there exist a natural band gap, while for $N = 3M + 2$, the gap is induced by hydrogen passivation. In Figure 3c, we show the corresponding relationship between the HOMO and LUMO positions and the lattice dilation, with slope determining the deformation potential E_1. For $N = 3M$, the E_1 for hole is about one order of magnitude larger than for electron. The situations for $N = 3M + 1$ and $N = 3M + 2$ are very similar but the E_1 for electrons is about one order of magnitude larger than that for holes. This phenomena originates from the nature of HOMO/LUMO for different N-AGNR. As shown in Figure 3d, for $N = 3M$, along the lattice dilation x-direction, the HOMO is of anti-bonding character, while the LUMO is of bonding character. However, for $N = 3M + 1$ it is just the reverse ($N = 3M + 2$ is the same as $N = 3M + 1$). Upon lattice dilation, bonding state is stable with respect to a structural change, and anti-bonding is unstable. Namely, the former represents a smaller deformation potential than the latter case. According to Equation (7), the mobility is inversely proportional to the square of E_1. Since the elastic constant C gradually changes with N, the calculated mobilities for electrons and holes exhibit strong fluctuating character and differ by two orders of magnitude (Figure 3e). Such size-dependent polarity suggests graphene nanoribbons are promising candidates for intrinsic p–n junctions through nanoengineering.

5. Conclusions and Outlook

Modeling carrier mobilities in organic and carbon materials presents a great challenge because of the complexity in the carrier-scattering mechanism, which is intrinsically a many-body problem. We present three approaches to computing the room-temperature charge mobility for organic and carbon materials at the first-principles level:

i) Hopping mobility through electron transfer rate plus a random walk simulation. Here, molecular parameters such as intermolecular electronic coupling and molecular reorganization

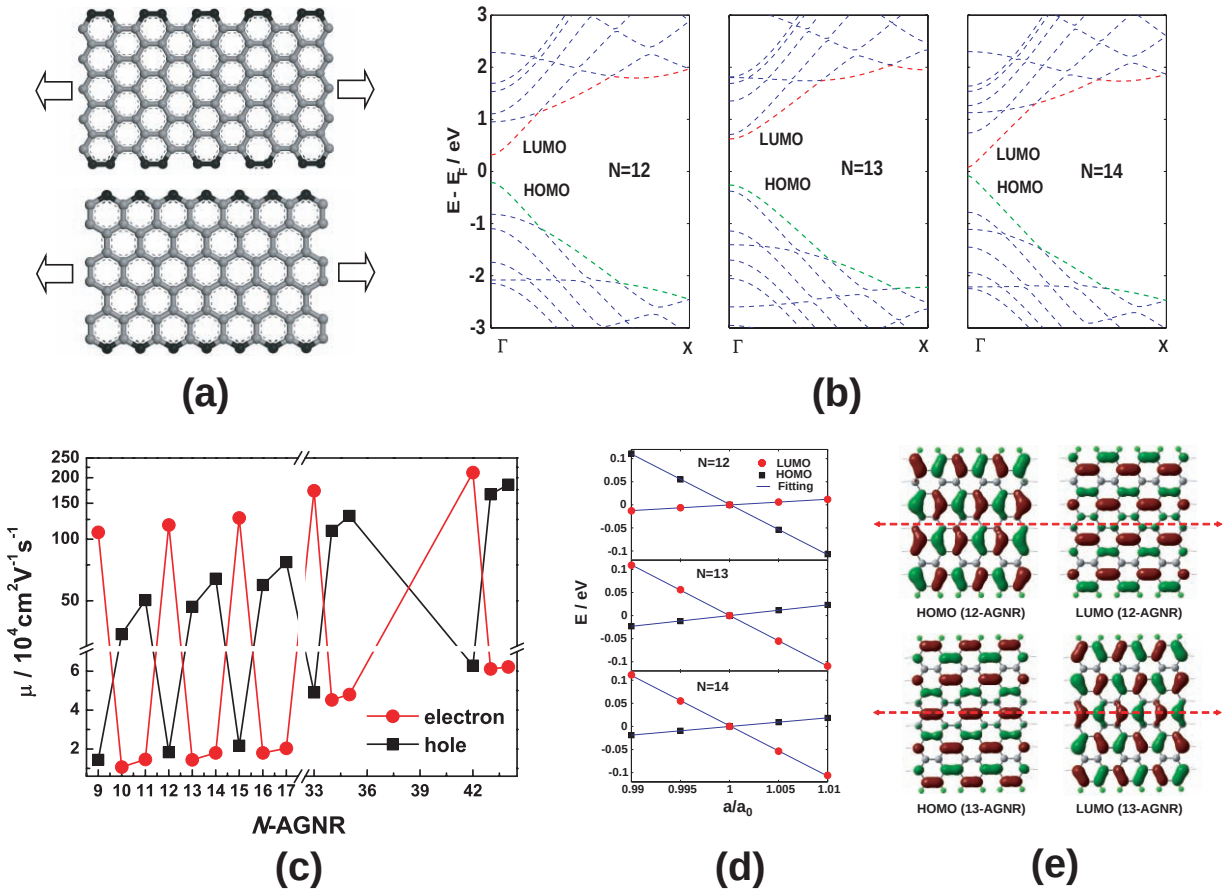

Figure 3. a) Schematic representation of the armchair- (top) and zig-zag- (bottom) edged graphene nanoribbons. The black atoms express the atoms at the edge. The arrows are the stretching directions. b) DFT band structures for *N*-AGNR (*N* = 12, 13, and 14). The green and red dashed lines indicate the HOMO and LUMO bands, respectively. c) The band edge shifts of the bottom of conduction band and the top of valence band as a function of deformation proportion for *N* = 12, 13, and 14. d) The isosurface plots of the *Γ*-point wave functions of HOMO and LUMO for 12-AGNR and 13-AGNR. The red dashed line stands for the direction of stretching. e) Calculated hole and electron mobility dependence on the width of the *N*-AGNR. Reproduced with permission.[30] Copyright 2009, ACS.

energy are calculated by quantum chemistry and the molecular packing structure serves as transport network for the particle diffusion simulation. The basic assumption is that the charge is localized in one molecule thus the major scattering arises from the intramolecular vibration. This approach has been widely applied to molecular design. The application range is $V \ll \lambda$, namely, that the intermolecular electron transfer integral is much less than the charge reorganization energy. Besides, the dynamic disorder arising from intermolecular vibrations was found to be unimportant for charge transport in such description.

ii) Polaron transport as described by the Holstein–Peierls model with parameters obtained and projected from DFT band structure calculation was found to be band-like for naphthalene crystals. In this case, the intermolecular vibrations are the major scattering source. Along the weak coupling *c*′-axis, it is found that for electron transport, there exhibit a band to hopping crossover as the temperature is increased to about 150 K, in excellent agreement with experiments. The overall calculated charge mobility overestimates the experimental results by one to two orders of magnitude. Here, a polaron allows some extend of charge delocalization. It can in principle give both band and hopping description. However, it overestimates both the band behavior and the mobility value.

iii) For well-delocalized electrons, much as for traditional inorganic semiconductors, the deformation potential theory is modeled as homogenous lattice dilation to approximate the acoustic phonon scattering. It turns out that the key parameters for transport are the elastic constant and the deformation potential measured as the first-order derivative of band edge position with respective to the lattice dilation, in addition to the effective mass. When applied to modeling graphene nanoribbons, we found that the polarity of carrier is dependent on the ribbon width when the ribbon edge is arm-chair, but not for zigzag edges. For arm chair-edged ribbon, there exists a periodicity of 3 along the edge. The polarity of transport arises from the frontier orbital's bonding and anti-bonding character along the charge transport direction.

There is no doubt that, driven by the remarkable advances in materials and devices, our understanding of carrier transport is moving rapidly towards a quantitative description

of charge mobility through comprehensive consideration of electron–phonon scatterings, from the usual one effective phonon mode approximation to all intra- and inter-molecular vibrations, as well as including both acoustic and optical phonons. Such understanding will be improved with high level treatment of the many-body problem and with electronic structure theory for weak intermolecular interactions,[56] as well as with advances in computational technology. We note that even for silicon, the most common electronic materials marketed for more than half a century, a quantitative understanding through first-principles calculations of electron–phonon scattering competing with impurity scattering was only made possible very recently.[57] By and large, phonon scattering is much too complicated for the computational materials sciences, but very essential for transport. Organic materials are complex systems compared to inorganic semiconductors. It is a formidable and necessary task to get quantitative description for charge transport in organic electronic materials, in order to help materials design. There is still a long way to go.

Acknowledgements

Essential contributions to this work from Drs. Xiaodi Yang, Guangjun Nan, Mengqiu Long, and Ling Tang are greatly acknowledged. The work was supported by the National Natural Science Foundation of China (grant nos. 20833004 and 20920102031) and the Ministry of Science and Technology through the 973 program (grant nos. 2009CB623600, 2011CB932304, and 2011CB808405).

Received: September 25, 2010
Published online: December 22, 2010

[1] a) G. Horowitz, *Adv. Mater.* **1998**, *10*, 365; b) V. Coropceanu, J. Cornil, D. A. Da Silva Filho, Y. Olivier, R. J. Silbey, J. L. Brédas, *Chem. Rev.* **2007**, *107*, 926.
[2] W. F. Beadle, J. C. C. Tsai, R. D. Plummer, (eds.), *Quick Reference Manual of Semiconductor Engineers*, Wiley, New York **1985**.
[3] a) A. Javey, J. Guo, Q. Wang, M. Lundstrom, H. Dai, *Nature (London)* **2003**, *424*, 654; b) J. Appenzeller, J. Knoch, V. Derycke, R. Martel, S. Wind, P. Avouris, *Phys. Rev. Lett.* **2002**, *89*, 126801; c) C. Berger, Z. Song, X. Li, X. Wu, N. Brown, C. Naud, D. Mayou, T. Li, J. Hass, A. N. Marchenkov, E. H. Conrad, P. N. First, W. A. de Heer, *Science* **2006**, *312*, 1191.
[4] a) A. J. Heeger, N. S. Sariciftci, E. B. Namdas, *Semiconducting and Metallic Polymers*, Oxford University Press, New York **2010**; b) Z. Bao, J. Locklin (eds.), *Organic Field Effect Transistors*, Taylor and Francis, Boca Raton, **2007**; c) G. Hadziioannou, G. G. Mallarias (eds.), *Semiconducting Polymers*, Wiley-VCH, Weinheim, **2007**; d) H. Klauk (ed.), *Organic Electronics*, Wiley-VCH, Weinheim, **2006**.
[5] C. R. Newman, C. D. Frisbie, D. A. da Silva Filho, J. L. Brédas, P. C. Ewbank, K. R. Mann, *Chem. Mater.* **2004**, *16*, 4436.
[6] a) V. C. Sundar, J. Zaumseil, V. Podzorov, E. Menard, R. L. Willett, T. Someya, M. E. Gershenson, J. A. Rogers, *Science* **2004**, *303*, 1644; b) V. Podzorov, E. Menard, A. Borissov, V. Kiryukhin, J. A. Rogers, M. E. Gershenson, *Phys. Rev. Lett.* **2004**, *93*, 086602.
[7] T. Holstein, *Ann. Phys. (N.Y.)* **1959**, *8*, 325.
[8] a) H. Bässler, *Phys. Status Solidi B* **1993**, *175*, 15; b) H. Bässler, G. Schonherr, M. Abkowitz, D. M. Pai, *Phys. Rev. B* **1982**, *26*, 3105; c) H. Bässler, *Philos. Mag. B* **1984**, *50*, 347.
[9] a) A. Dieckmann, H. Bässler, P. M. Borsenberger, *J. Chem. Phys.* **1993**, *99*, 8136; b) P. M. Borsenberger, J. J. Fitzgerald, *J. Phys. Chem.* **1993**, *97*, 4815.
[10] M. E. Gershenson, V. Podzorov, A. F. Morpurgo, *Rev. Mod. Phys.* **2006**, *78*, 973.
[11] a) J. L. Brédas, J. P. Calbert, D. A. da Silva, J. Cornil, *Proc. Natl. Acad. Sci. U.S.A.* **2002**, *99*, 5804; b) J. Cornil, D. Beljonne, J. P. Calbert, J. L. Brédas, *Adv. Mater.* **2001**, *13*, 1053; c) J. L. Brédas, D. Beljonne, V. Coropceanu, J. Cornil, *Chem. Rev.* **2004**, *104*, 4971.
[12] J. E. Norton, J. L. Brédas, *J. Am. Chem. Soc.* **2008**, *130*, 12377.
[13] a) R. W. Munn, R. Silbey, *J. Chem. Phys.* **1985**, *83*, **1854**; b) R. Silbey, R. W. Munn, *J. Chem. Phys.* **1980**, *72*, 2763.
[14] V. M. Kenkre, J. D. Anderson, D. H. Dunlap, C. B. Duck, *Phys. Rev. Lett.* **1989**, *62*, 1165.
[15] a) K. Hannewald, P. A. Bobbert, *Appl. Phys. Lett.* **2004**, *85*, 1535; b) K. Hannewald, V. M. Stojanovic, J. M. T. Schellekens, P. A. Bobbert, G. Kresse, J. Hafner, *Phys. Rev. B* **2004**, *69*, 075212; c) K. Hannewald, V. M. Stojanovic, P. A. Bobbert, *J. Phys.: Condens. Matter* **2004**, *16*, 2023.
[16] M. Hultell, S. Stafström, *Chem. Phys. Lett.* **2006**, *428*, 446.
[17] a) A. Troisi, G. Orlandi, *Phys. Rev. Lett.* **2006**, *96*, 086601; b) A. Troisi, *Adv. Mater.* **2007**, *19*, 2000.
[18] L. J. Wang, G. J. Nan, X. D. Yang, Q. Peng, Q. K. Li, Z. G. Shuai, *Chem. Soc. Rev.* **2010**, *39*, 423.
[19] S. W. Yin, Y. P. Yi, Q. X. Li, G. Yu, Y. Q. Liu, Z. G. Shuai, *J. Phys. Chem. A*, **2006**, *110*, 7138.
[20] Y. B. Song, C. A. Di, X. D. Yang, S. P. Li, W. Xu, Y. Q. Liu, L. M. Yang, Z. G. Shuai, D. Q. Zhang, D. B. Zhu, *J. Am. Chem. Soc.* **2006**, *128*, 15940.
[21] X. D. Yang, Q. K. Li, Z. G. Shuai, *Nanotech.* **2007**, *18*, 424029.
[22] L. Q. Li, H. X. Li, X. D. Yang, W. P. Hu, Y. B. Song, Z. G. Shuai, W. Xu, Y. Q. Liu, D. B. Zhu, *Adv. Mater.* **2007**, *19*, 2613.
[23] G. J. Nan, X. D. Yang, L. J. Wang, Z. G. Shuai, Y. Zhao, *Phys. Rev. B* **2009**, *79*, 115203.
[24] X. D. Yang, L. J. Wang, C. L. Wang, W. Long, Z. G. Shuai, *Chem. Mater.* **2008**, *20*, 3205.
[25] L. J. Wang, Q. K. Li, Z. G. Shuai, L. P. Chen, Q. Shi, *Phys. Chem. Chem. Phys.* **2010**, *12*, 3309.
[26] L. J. Wang, Q. Peng, Q. K. Li, Z. G. Shuai, *J. Chem. Phys.* **2007**, *127*, 044506.
[27] L. J. Wang, Q. K. Li, Z. G. Shuai, *J. Mol. Sci.* (in Chinese) **2008**, *24*, 133.
[28] L. J. Wang, Q. K. Li, Z. G. Shuai, *J. Chem. Phys.* **2008**, *128*, 194706.
[29] L. Tang, M. Q. Long, D. Wang, Z. G. Shuai, *Sci. China, Ser. B: Chem.* **2009**, *52*, 1646.
[30] M. Q. Long, L. Tang, D. Wang, L. J. Wang, Z. G. Shuai, *J. Am. Chem. Soc.* **2009**, *131*, 224704.
[31] T. Holstein, *Ann. Phys. (N.Y.)* **1959**, *8*, 343.
[32] a) A. Troisi, G. Orlandi, *Chem. Phys. Lett.* **2001**, *344*, 509; b) B. C. Lin, C. P. Cheng, Z. Q. You, C. P. Hsu, *J. Am. Chem. Soc.* **2005**, *127*, 66.
[33] D. A. da Silva Filho, V. Coropceanu, D. Fichou, N. E. Gruhn, T. G. Bill, J. Gierschner, J. Cornil, J. L. Brédas, *Philos. Trans. R. Soc. A* **2007**, *365*, 1435.
[34] V. Lemaur, D. A. Da Silva Filho, V. Coropceanu, M. Lehmann, Y. Geerts, J. Piris, M. G. Debije, A. M. Van de Craats, K. Senthilkumar, L. D. A. Siebbeles, J. M. Warman, J. L. Brédas, J. Cornil, *J. Am. Chem. Soc.* **2004**, *126*, 3271.
[35] W. Q. Deng, W. A. Goddard, III, *J. Phys. Chem. B* **2004**, *108*, 8614.
[36] G. R. Hutchison, M. A. Ratner, T. J. Marks, *J. Am. Chem. Soc.* **2005**, *127*, 16866.
[37] G. Horowitz, D. Fichou, X. Z. Peng, Z. G. Xu, F. Garnier, *Solid State Commun.* **1989**, *72*, 381.
[38] C. Kloc, P. G. Simpkins, T. Siegrist, R. A. Laudise, *J. Cryst. Growth* **1997**, *182*, 416.
[39] a) H. E. Katz, L. Torsi, A. Dodabalapur, *Chem. Mater.* **1995**, *7*, 2235; b) R. Hajlaoui, D. Fichou, G. Horowitz, B. Nessakh, M. Constant, F. Garnier, *Adv. Mater.* **1997**, *9*, 557; c) R. Hajlaoui, G. Horowitz,

F. Garnier, A. Arce-Brouchet, L. Laigre, A. Elkassmi, F. Demanze, F. Kouki, *Adv. Mater.* **1997**, *9*, 389.
[40] B. Servet, G. Horowitz, S. Ries, O. Lagorsse, P. Alnot, A. Yassar, F. Deloffre, P. Srivastava, R. Hajlaoui, P. Lang, F. Garnier, *Chem. Mater.* **1994**, *6*, 1809.
[41] H. Sun, *J. Phys. Chem. B* **1998**, *102*, 7338.
[42] G. D. Mahan, *Many-Particle Physics*, 3rd ed., Kluwer Academic/ Plenum Publisher, New York **2000**.
[43] N. Karl, *Synth. Met.* **2003**, *133*, 649.
[44] a) G. Kresse, J. Hafner, *Phys. Rev. B* **1993**, *47*, 558; b) *G. Kresse, J. Hafner, Phys. Rev. B* **1994**, *49*, 14251; c) G. Kresse, J. Furthmüller, *Phys. Rev. B* **1996**, *54*, 11169.
[45] J. P. Perdew, K. Burke, M. Ernzerhof, *Phys. Rev. Lett.* **1996**, *77*, 3865.
[46] E. F. C. Byrd, G. E. Scuseria, C. F. Chabalowski, *J. Phys. Chem. B* **2004**, *108*, 13100.
[47] V. I. Ponomarev, O. S. Filipenko, L. O. Atovmyan, *Crystallogr. Rep.* **1976**, *21*, 392.
[48] a) T. Kato, T. Yamabe, *J. Chem. Phys.* **2001**, *115*, 8592; b) L. B. Schein, C. B. Duck, A. R. McGhie, *Phys. Rev. Lett.* **1978**, *40*, 197.
[49] J. Bardeen, W. Shockley, *Phys. Rev.* **1950**, *80*, 72.
[50] a) Y. C. Cheng, R. J. Silbey, D. A. da Silva Filho, J. P. Calbert, J. Cornil, J. L. Brédas, *J. Chem. Phys.* **2003**, *118*, 3764; b) J. M. Ziman, *Principles of the Theory of Solids*, 2nd ed., Cambridge University Press, London **1972**, pp. 211–229.
[51] a) F. B. Beleznay, F. Bogar, J. Ladik, *J. Chem. Phys.* **2003**, *119*, 5690; b) R. A. Street, J. E. Northrup, A. Salleo, *Phys. Rev. B* **2005**, *71*, 165202.
[52] J. Ladik, G. Biczo, G. Elek, *J. Chem. Phys.* **1966**, *44*, 483.
[53] a) N. Y. Sa, G. Wang, B. Yin, Y. H. Huang, *Phys. E*, **2008**, *40*, 2396; b) B. Xu, Y. D. Xia, J. Yin, X. G. Wan, K. Jiang, A. D. Li, D. Wu, Z. G. Liu, *Appl. Phys. Lett.* **2010**, *96*, 183108.
[54] a) K. S. Novoselov, A. K. Geim, S. V. Morozov, D. E. Jiang, Y. Zhang, S. V. Dubonos, I. V. Grigorieva, A. A. Firsov, *Science* **2004**, *306*, 666; b) J. S. Bunch, A. M. van der Zande, S. S. Verbridge, I. W. Frank, D. M. Tanenbaum, J. M. Parpia, H. G. Craighead, P. L. McEuen, *Science* **2007**, *315*, 490; c) M. Y. Han, B. Özyilmaz, Y. Zhang, P. Kim, P. *Phys. Rev. Lett.* **2007**, *98*, 206805.
[55] a) C. Berger, Z. Song, X. Li, X. Wu, N. Brown, C. Naud, D. Mayou, T. Li, J. Hass, A. N. Marchenkov, E. H. Conrad, P. N. First, W. A. de Heer, *Science* **2006**, *312*, 1191; b) P. Neugebauer, M. Ortila, C. Faugeras, A. L. Bara, M. Potemski, *Phys. Rev. Lett.* **2009**, *103*, 136403.
[56] a) A. J. Cohen, P. Mori-Sanchez, W. Yang, *Science* **2008**, *321*, 792; b) A. J. Stone, *Science* **2008**, *321*, 787.
[57] a) J. Sjakste, N. Vast, V. Tyuterev, *Phys. Rev. Lett.* **2007**, *99*, 236405; b) O. D. Restrepo, K. Varga, S. T. Pantelides, *Appl. Phys. Lett.* **2009**, *94*, 212103; c) V. Lordi, P. Erhart, D. Åberg, *Phys. Rev. B* **2010**, *81*, 235204.